

Tuning the Selective Permeability of Polydisperse Polymer Networks

Won Kyu Kim,^{1,*} Richard Chudoba,^{2,3} Sebastian Milster,^{2,4}
Rafael Roa,⁵ Matej Kanduč,⁶ and Joachim Dzubiella^{2,4,7,†}

¹*Korea Institute for Advanced Study, Seoul 02455, Republic of Korea*

²*Research Group for Simulations of Energy Materials,
Helmholtz-Zentrum Berlin für Materialien und Energie, D-14109 Berlin, Germany*

³*Division of Theoretical Chemistry, Department of Chemistry,
Lund University, P.O. Box 124, SE-22100 Lund, Sweden*

⁴*Applied Theoretical Physics-Computational Physics, Physikalisches Institut,
Albert-Ludwigs-Universität Freiburg, D-79104 Freiburg, Germany*

⁵*Departamento de Física Aplicada I, Facultad de Ciencias, Universidad de Málaga, E-29071 Málaga, Spain*

⁶*Jožef Stefan Institute, SI-1000 Ljubljana, Slovenia*

⁷*Cluster of Excellence livMatS @ FIT - Freiburg Center for Interactive Materials and Bioinspired Technologies,
Albert-Ludwigs-Universität Freiburg, D-79110 Freiburg, Germany*

(Dated: April 18, 2020)

We study the permeability and selectivity (‘permselectivity’) of model membranes made of polydisperse polymer networks for molecular penetrant transport, using coarse-grained, implicit-solvent computer simulations. The permeability \mathcal{P} is determined on the linear-response level using the solution–diffusion model, $\mathcal{P} = \mathcal{K}D_{\text{in}}$, *i.e.*, by calculating the equilibrium penetrant partition ratio \mathcal{K} and penetrant diffusivity D_{in} inside the membrane. We vary two key parameters, namely the monomer–monomer interaction, which controls the degree of swelling and collapse of the network, and the monomer–penetrant interaction, which tunes the penetrant uptake and microscopic energy landscape for diffusive transport. The results for the partition ratio \mathcal{K} cover four orders of magnitude and are non-monotonic versus the parameters, which is well interpreted by a second-order virial expansion of the free energy of transferring one penetrant from bulk into the polymeric medium. We find that the penetrant diffusivity D_{in} in the polydisperse networks, in contrast to highly ordered membrane structures, exhibits relatively simple exponential decays and obeys well-known free-volume and Kramers’ escape scaling laws. The eventually resulting permeability \mathcal{P} thus resembles the qualitative functional behavior (including maximization and minimization) of the partitioning. However, partitioning and diffusion are anti-correlated, yielding large quantitative cancellations, controlled and fine-tuned by the network density and interactions as rationalized by our scaling laws. As a consequence, we finally demonstrate that even small changes of penetrant–network interactions, *e.g.*, by half a $k_{\text{B}}T$, modify the permselectivity of the membrane by almost one order of magnitude.

I. INTRODUCTION

Being a key transport property in materials science, the *permeability* of membranes has been excessively studied for more than a century [1–5]. The permeability determines the fundamental ability of functional solutes such as ions, ligands, proteins, and reactants to penetrate and be transported through dense but permeable membranes of various kinds. Membranes constitute typically quite crowded environments, are mostly polymer-based, and are ubiquitous in soft matter applications, materials science, and naturally in biological systems. In the latter, bio-hydrogels such as cytoskeletons, mucus gels, and the extracellular matrix (ECM) are complex molecular assemblies composed of hydrated polymer networks [4, 6–11] in cells. In general, they function as selectively permeable barriers for solutes to penetrate [9]. For instance, ECM constructs a selective barrier around the cells, thereby regulating transport of sig-

naling molecules [9, 12–18]. Hence, the permeability of bio-hydrogels plays a decisive role in maintaining life.

Other important examples of polymer-network-based membranes can be found in functional soft matter composed of synthetic hydrogels, such as cross-linked poly(*N*-isopropylacrylamide) (PNIPAM) [19]. Due to their thermoresponsiveness and relatively sharp volume transition they are widely used as representative and promising components in emerging material technologies for stimuli-responsive carrier particles, actuators, sensors, or responsive nanoreactors [20–33]. In the latter, for instance, the hydrogel embeds nano-sized enzymes or metal nanoparticles catalyzing chemical reactions, which are ultimately controlled by the responsive membrane permeability [34–36]. In general, responsive polymeric matrices can be expected to control permeation of (co)solute penetrants in a selective manner, modulated by external stimuli such as temperature, pH, and salinity. The tunable selectivity of the permeability (‘permselectivity’) [4] thus bears enormous potential for the development of ‘intelligent’, programmable and adaptive membranes for diverse applications ranging from gas separation [37–43], water purification, and filtration [44–

* wonkyukim@kias.re.kr

† joachim.dzubiella@physik.uni-freiburg.de

50] to dialysis and drug delivery [51, 52].

Typically, the permeability of dense membranes is quantified by the so-called solution-diffusion model on a linear-response level, via [3, 5, 37, 38, 43, 53–60]

$$\mathcal{P} = \mathcal{K}D_{\text{in}}, \quad (1)$$

that is, it is the product of two key equilibrium quantities, namely the partitioning (partition ratio) $\mathcal{K} = c_{\text{in}}/c_0$, simply given by the ratio between the penetrant concentrations inside the membrane c_{in} and in the bulk c_0 , and the diffusivity (diffusion coefficient) D_{in} of the penetrants inside the membrane. The permeability of the bulk reference is thus equal to the free penetrant diffusivity in the bulk, *i.e.*, $\mathcal{P}_0 = D_0$. The elegance of Eq. 1 is, that it is simply based on two intuitive and fundamental equilibrium properties of a medium, which should be presumably easy to access experimentally and theoretically tractable.

However, there is a still growing number of theoretical studies pursuing a better understanding of partitioning [39–41, 61–68] and diffusivity [37, 53, 55, 56, 69–91] in polymer-based membranes and hydrogels. It is the complexity arising from diverse molecular interactions (*e.g.*, excluded volume and attraction) and conformational structures (cross-linked, ordered, polydisperse) inside the membrane that renders the problem very challenging. In this context, for instance, we recently presented a simple coarse-grained (CG) simulation model of penetrant transport across a rigid immobile lattice-based membrane, pursuing a better comprehension of the permeability particularly in dense and attractive systems [84]. Despite the simplicity of that model, we demonstrated a very intricate behavior of the permeability: the latter varied over many orders of magnitude, and could even be minimized or maximized by tailoring the potential energy landscape for the diffusing penetrants through small variations of membrane attraction, structure, and density. Supported by limiting scaling theories, we showed that the possible occurrence of extreme values is far from trivial, being evoked by a strong anti-correlation and substantial (orders of magnitude) cancellation between penetrant partitioning and diffusivity, especially in the case of dense and highly attractive membranes.

In this work, we extend the previous study of a fixed, ordered membrane topology to a more complex and more realistic case of a membrane composed of fluctuating and cross-linked *polydisperse* polymers to study the transport of diffusive penetrants. For this, we consider a polydisperse tetra-functional network, *i.e.*, each cross-linker connects four polymer strands, which have a polydisperse length distribution. As similarly considered previously [66, 84], the system includes the network region and the bulk region, enabling a direct calculation of partitioning, diffusivity, and thus permeability. We focus on two important control parameters: the polymer network density ϕ_n (volume fraction), tuned by internal interactions, and the interaction between the network

monomers and the penetrants. We calculate the linear response permeability \mathcal{P} according to eqn (1) and systematically analyze and rationalize our findings by presenting semi-empirical scaling laws. Finally, we demonstrate how minute changes of the interactions can modify the permselectivity of the membrane substantially.

II. METHODS

A. Simulation model

1. Network structure and setup

We performed implicit-solvent Langevin dynamics computer simulations of the model membrane made of a polydisperse polymer network [92–95] including diffusive penetrants (see Fig. 1a), where each cross-linker connects four polymer chains but with different chain lengths. For the initial configuration of the network we considered $4 \times 4 \times 4$ unit cells of a diamond cubic lattice, where $N_x = 64 \times 8 = 512$ cross-linkers were located on the lattice points. The number of polymer monomers between the (closest neighboring) cross-linkers was randomly drawn from a uniform distribution between 2 and 18, thereby resulting in the polydisperse structure with an average chain length of 10 monomers, and a standard deviation of about 5. With the above construction we ended up with $N_m = 10364$ monomers in the network, yielding a cross-linker fraction of $f_x = 4.7\%$. This cross-linker fraction is in the range of typical experimental values for tetra-functional polymer networks, such as cross-linked PNIPAM hydrogels [85–89].

For initial equilibration, the membrane was placed in the middle of a simulation box of lateral lengths $L_x = L_y = 100\sigma$ (with σ defining the penetrant size and our length scale) and the longitudinal length $L_z = 300\sigma$, with periodic boundary conditions in all three Cartesian directions. The membrane was first equilibrated in the NVT ensemble in the presence of the force-field described below. We then added $N_p = 1000$ penetrant particles into the bulk region, and equilibrated the whole system. In the next step, the longitudinal box length L_z was kept fixed, while L_x and L_y could adjust according to the NpT ensemble with a given particle number $N = N_m + N_x + N_p = 11876$, pressure $p_x = p_y = p$, and temperature T . The system was then finally allowed to equilibrate again before finally gathering statistics in the production runs.

Selected two-dimensional radial density distribution functions between the cross-linkers $g_{\text{xx}}^{2\text{D}}(r)$, shown in Fig. 2, demonstrate that the equilibration procedure leads to reasonable and homogeneous network structures (the $g_{\text{xx}}^{2\text{D}}(r)$ is averaged over thin two-dimensional membrane slabs in xy -directions, see the Electronic Supplementary Information (ESI) for details). Especially in the dense state, apart for some short-ranged packing effects, for $r \gtrsim 3\sigma$ the system is very homogeneous. For the

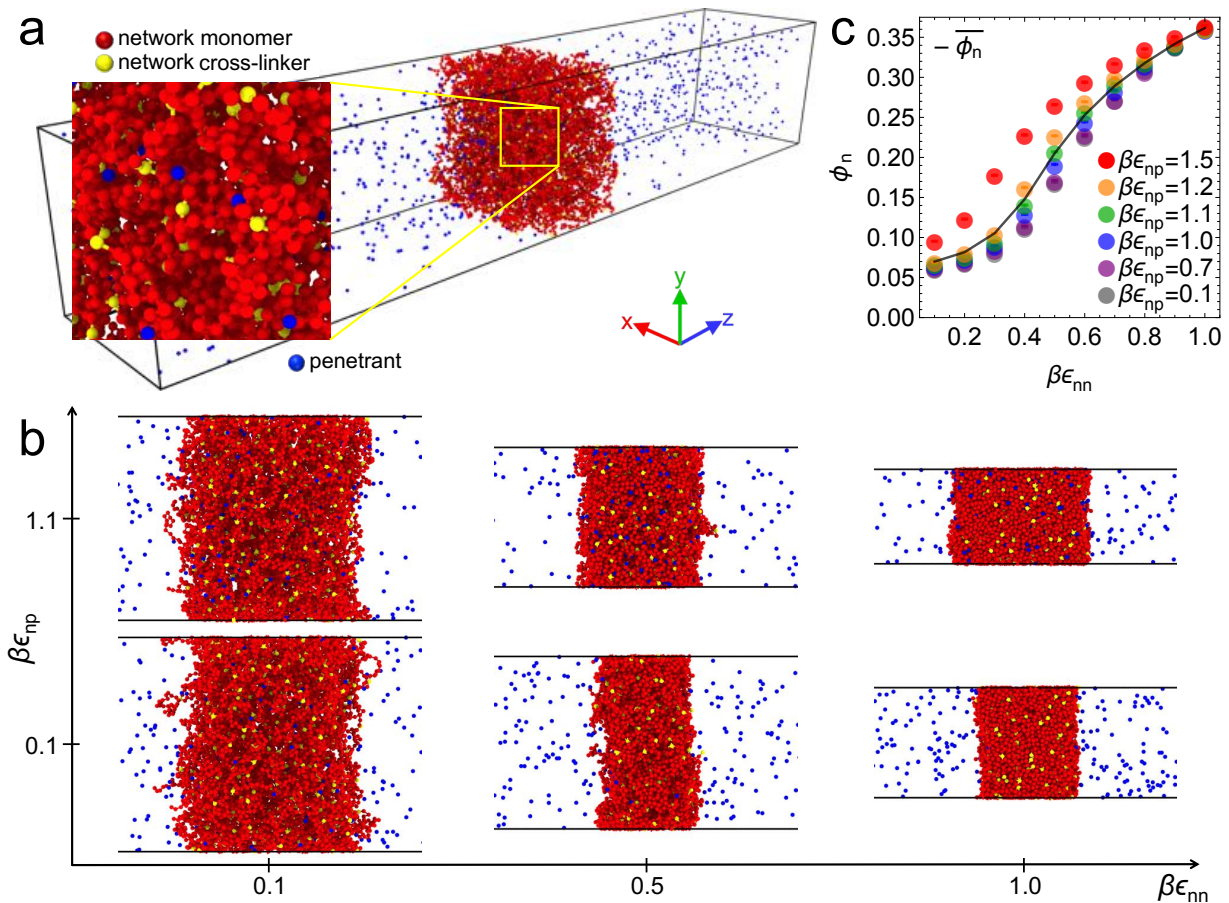


FIG. 1. (a) Simulation snapshot of the polydisperse tetra-functional polymer network in the swollen state with diffusive penetrants (blue). The polymer segments (red beads) are connected by tetra-functional cross-linkers (yellow beads) and have a random length distribution (see text in Methods). (b) Various network conformations depending on ϵ_{nn} and ϵ_{np} . The network collapses as the the network–network interaction parameter ϵ_{nn} increases (*i.e.*, lowering the solvent quality to poor solvent conditions). (c) The polymer network volume fractions ϕ_n vs. the solvent quality parameter ϵ_{nn} at different values of the network–penetrant parameters ϵ_{np} (see text for details). The solid line depicts the mean volume fraction $\bar{\phi}_n(\epsilon_{nn})$ interpolating between the averages over all simulated ϵ_{np} values.

swollen network, $g_{xx}^{2D}(r)$ reveals some more structure with a local peak in $3\sigma \lesssim r \lesssim 4\sigma$, reflecting short-range correlations between the crowded cross-linker regions, and a second peak close to the average chain length (*i.e.*, average mesh size in the swollen case) of $r \simeq 10\sigma$. Changing the network–penetrant interaction affects these distributions only slightly in the dense systems, while in the swollen case some homogenization is observed for large attractions between the network and the penetrants (see Fig. S1 in ESI).

As described in our previous studies [66, 84], we employed the LAMMPS software [96] with the stochastic Langevin integrator in the NpT ensemble. To maintain fixed pressure, we used the Berendsen anisotropic barostat [97]. The iteration time step $\delta\tau = 5 \times 10^{-3}\tau$ was used with the time units $\tau = \sqrt{m\sigma^2/k_B T}$, where m is the unit mass, and $k_B T = 1/\beta$ is the thermal energy. The friction coefficient γ was chosen to have the momentum relaxation time $\tau_\gamma = m/\gamma = \tau$, so that the

free penetrants' motion becomes diffusive after 200 time steps. The value of the lateral pressure was chosen to be $p = 6.5853 \times 10^{-4} k_B T/\sigma^3 \approx 1$ bar. The pressure relaxation time τ_p and bulk modulus K_b for the barostat were carefully chosen in the range of $1 \leq \tau_p/\tau \leq 2$ and $1 \leq K_b/p \leq 10$, respectively, depending on the interaction parameters. After an equilibration time of $1.5 \times 10^5 \tau$, we performed the production simulations typically up to $10^7 \delta\tau = 5 \times 10^4 \tau$. As the finite network membrane is connected to the large bulk region of solute penetrants, the simulations are effectively isobaric/semi-grand canonical in the sense that the penetrants can always equilibrate their partitioning between the large bulk and the (responsive) membrane, subjected to the constant lateral pressure.

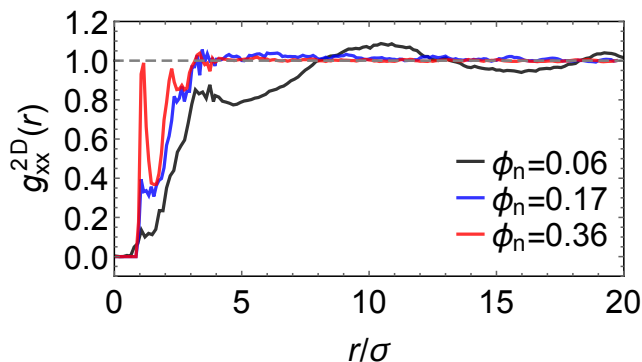


FIG. 2. The two-dimensional radial distribution function between the cross-linkers $g_{xx}^{2D}(r)$ for three different polymer volume fractions, from swollen ($\phi_n = 0.06$) to collapsed ($\phi_n = 0.36$) states. The network–penetrant interaction parameter is $\beta\epsilon_{np} = 0.1$. The distribution function $g_{xx}^{2D}(r)$ is averaged over thin 2D membrane slabs in xy -directions, see ESI for details and more data.

2. Force field

For the non-bonded interactions, all particles (i.e., monomer, crosslinker, penetrant beads) interact via the generic Lennard-Jones (LJ) potential U_{LJ}^{ij} for $i, j = n$ or p , where n denotes the network particles (polymer monomers and cross-linkers), and p denotes the penetrant. The strength $\epsilon_{pp} = 0.1 k_B T$ of the LJ potential U_{LJ}^{pp} is fixed such that the penetrants are overall repulsive [66, 84] (see also the positive second virial coefficient of the LJ interaction plotted in Fig. S2a in ESI, and the following sections for details of the virial coefficients). In this work we vary two interaction parameters, the network–network interaction ϵ_{nn} , and the network–penetrant interaction ϵ_{np} , between 0.1 and 1.5 $k_B T$. The intra-network interaction ϵ_{nn} is interpreted as a measure of solvent quality [66, 84, 98], thereby controlling the network volume fraction ϕ_n . As discussed in previous works [66, 84, 98], small/high ϵ_{nn} corresponds to good/poor solvent leading to a small/high volume fraction, respectively. The network–penetrant interaction ϵ_{np} governs the strength of the attraction between the polymers and the penetrants.

For the bonded interactions of the (semi-flexible) polymers we employed harmonic stretching (bonds) and bending (angles) potentials [66]. The bonded polymer parameters were determined via coarse-graining from explicit-water, all-atom simulation results of cross-linked PNIPAM chains, utilizing a force-field from our group’s work [99]. Since the cross-linker (x) connects monomers (m) of four polymer chains, the network is tetra-functional, and in addition to the m-m-m bending, there are six bending potentials for the m-x-m arrangement. Therefore, we have nine different bonding (7 bending (angles), 2 stretching (bonds)) potentials in total and we determined eighteen bond parameters K_r^{ij} , r_0^{ij} , K_θ^{ijk} ,

and θ_0^{ijk} by fitting harmonic potentials to the free energies obtained from the all-atom simulations. The details of all the bonded interactions, that is, their calculation from the all-atom (explicit-water) simulations of PNI-PAM and their final definition, can be found in ESI.

B. Analysis

The partition ratio, $\mathcal{K} = c_{in}/c_0$, was computed by counting and averaging the equilibrium number density of penetrants inside the network and bulk, as similarly done in our previous works [36, 66, 84]: we carefully divided the simulation box into three regions (inner membrane, membrane surface, and bulk) to sample the concentrations without any surface effects (due to the finite membrane width). See Fig. S3 ESI for details.

To calculate the penetrant diffusivity in the network, D_{in} , we generated 20 simulation boxes of diamond unit cells of the polydisperse tetra-functional networks including the penetrants for each parameter set of ϵ_{nn} and ϵ_{np} , and we performed additional simulations of these periodic cells (see Fig. S4 in ESI). To determine the cell size and the number of the penetrants in the cell, we used the equilibrium values of the penetrant density and the polymer density obtained from the main simulation data. We computed the mean-squared-displacement (MSD) of the penetrants in the networks, averaged over time and particles [100], as shown in supplementary Fig. S5 (upper panels), within the dimensionless simulation time range from $t = 100$ to $t = 1000$ to obtain diffusivity via $MSD = 6D_{in}t$, ensuring the normal diffusion [100], which fulfills $\alpha = \frac{d \ln MSD}{d \ln t} = 1$ in Fig. S5 (lower panels).

III. RESULTS AND DISCUSSION

A. Network density response to solvent quality and penetrants

Six representative simulation snapshots of the total system are shown in Fig. 1b for different values of the solvent quality parameter ϵ_{nn} and the network–penetrant interaction parameter ϵ_{np} . The most swollen state is shown by the lower left snapshot, whereas the most compact state is depicted by the upper right snapshot. The polymer network collapses due to strong network–network attractions ϵ_{nn} (poor solvent), otherwise it swells (good solvent). In addition, upon changing the network–penetrant interaction, particularly at the intermediate solvent quality ($\epsilon_{nn} = 0.5 k_B T$), we note that the larger the attraction ϵ_{np} , the more packed is the network (lower volume). This is due to bridging effects of highly attractive penetrant, contracting the network to maximize favorable interaction contacts [66]. See Fig. S6 in ESI for details of the network volume change depending on the interactions.

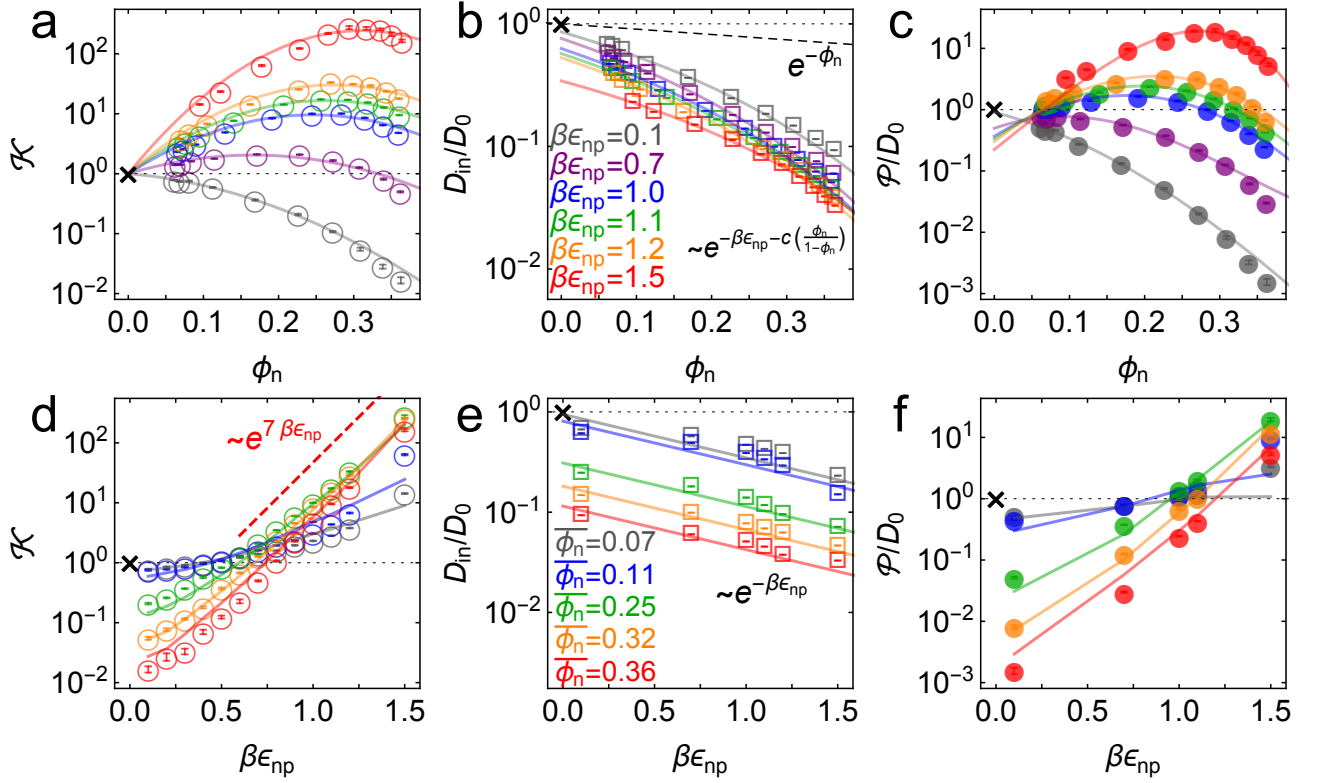


FIG. 3. Simulation results (symbols) and theoretical fits (solid lines) are shown. (a) Partitioning \mathcal{K} as a function of the network volume fraction for different values of the network–penetrant interaction ϵ_{np} . The solid lines are the fits from virial expansion Eq. (2) (see text and Table S1 in ESI for details). (b) Penetrant diffusion in the polymer network D_{in} as a function of ϕ_n . The solid lines are the fits (also depicted in (e)) from the free-volume approach Eq. (4) (see Table S2 in ESI for the details). The dashed line is $e^{-\phi_n}$ as a reference. (c) Permeability \mathcal{P} as a function of ϕ_n . The solid lines are the predictions from Eq. (5) using the fitting values from (a) and (b). (d) Partitioning \mathcal{K} as a function of ϵ_{np} . The solid lines are the prediction according to the virial expansion Eq. (2) using the B_2^{np} and B_3^{nnp} values from the fit in (a) and the mean density $\phi_n = \bar{\phi}_n$. The data scales roughly as $\mathcal{K} \sim e^{7\beta\epsilon_{np}}$ for dense and attractive polymers (red dashed line). (e) Penetrant diffusion D_{in} as a function of ϵ_{np} . The solid lines are the fits according to the exponential (Kramers’) scaling $D_{in}/D_0 \sim e^{-\beta\epsilon_{np}}$ from Eq. (4). (f) Permeability \mathcal{P} as a function of ϵ_{np} . The solid lines are the predictions from Eq. (5) using the fitting values from (a) (see also panels (d) and (e)). The cross symbols in each panel are corresponding reference values in the bulk.

The global effects of the two interaction parameters are summarized in Fig. 1c, which depicts the network volume fraction ϕ_n , *i.e.*, the ratio of the volume occupied by the polymers to the entire network volume, as a function of the solvent quality parameter ϵ_{nn} for different values of the network–penetrant interaction ϵ_{np} . The network undergoes a typical collapse transition as ϵ_{nn} increases at small and intermediate values of ϵ_{np} , while the transition becomes more gradual when the attraction is very high ($\epsilon_{np} = 1.5 k_B T$). This is probably due to local monomer clustering and network homogeneity, cf. Fig. S1, smoothing the transition. Note that in Fig. 1c we also depict the mean volume fraction $\bar{\phi}_n(\epsilon_{nn})$, which is the average over all simulated ϵ_{np} .

B. Penetrant partitioning, diffusivity, and permeability

1. Partitioning

In Fig. 3 we show the partitioning \mathcal{K} , the penetrant diffusion inside the network D_{in} , and the permeability \mathcal{P} , as a function of the network volume fraction (a–c) and the network–penetrant interaction parameter (d–e).

The partitioning as a function of the network volume fraction, $\mathcal{K}(\phi_n)$, exhibits diverse behavior, ranging over four orders of magnitude depending on the interactions, as shown in Fig. 3a. For low network–penetrant interaction parameters ϵ_{np} , \mathcal{K} is monotonically decreasing with increasing network density, since the essentially repelled penetrants are excluded by highly packed polymers (see the second virial coefficient of the LJ system shown in Fig. S2a in ESI). For higher values of the LJ potential depth ϵ_{np} , the penetrants are increasingly more attracted

TABLE I. Virial coefficients B_2^{np} and B_3^{np} in Eq. (2) obtained as fitting parameters in Fig. 2a are shown for different values of ϵ_{np} . The exact values of B_2^{LJ} and B_3^{LJ} for LJ potential are shown for comparison. The fitting parameter values b and c in the free-volume scaling theory Eq. (3) (see also Fig. 3b) are shown. See ESI for details.

$\beta\epsilon_{\text{np}}$	0.1	0.7	1.0	1.1	1.2	1.5
B_2^{np}/σ^3	0.63 ± 0.08	-2.25 ± 0.17	-4.82 ± 0.19	-5.61 ± 0.16	-6.52 ± 0.21	-9.26 ± 0.34
B_2^{LJ}/σ^3	0.97	-2.77	-5.32	-6.27	-7.29	-10.75
B_3^{np}/σ^6	3.85 ± 0.35	4.74 ± 0.44	6.85 ± 0.45	7.46 ± 0.38	8.31 ± 0.48	10.41 ± 0.74
B_3^{LJ}/σ^6	1.25	2.46	1.89	0.55	-1.92	-22.07
b	0.86 ± 0.02	0.76 ± 0.02	0.63 ± 0.02	0.57 ± 0.01	0.53 ± 0.02	0.34 ± 0.01
c	4.17 ± 0.19	4.81 ± 0.16	4.77 ± 0.19	4.69 ± 0.18	4.79 ± 0.20	3.87 ± 0.09

to the network. The partitioning \mathcal{K} , however, becomes non-monotonic and reaches a maximum around $\phi_n \simeq 0.3$. This partitioning maximization is due to the volume exclusion of the penetrants, which wins over the attraction at high densities [67, 84].

The cross-over from penetrant exclusion to enrichment for increasing ϵ_{np} at fixed polymer density ϕ_n becomes obvious in Fig. 3d, where we plot $\mathcal{K}(\epsilon_{\text{np}})$. At around $\beta\epsilon_{\text{np}} \simeq 0.5-0.7$ (depending in detail on polymer density) the attraction outvalues the steric obstruction and penetrants are on average preferentially adsorbed than being in bulk, *i.e.*, $\mathcal{K} > 1$. We also observe that the partitioning $\mathcal{K}(\epsilon_{\text{np}})$ exhibits roughly an exponential increase with larger slope as ϕ_n increases. The exponential increase of the partitioning is also found in ordered membranes [84], reflecting that the overall scaling behavior of partitioning (upon changing the interactions) is rather insensitive to the regularity of the network. For dense and attractive polymer networks, we empirically find that $\mathcal{K} \sim e^{7\beta\epsilon_{\text{np}}}$, as depicted in Fig. 3d. The prefactor 7 reflects the total mean attraction in the dense systems, where the potential wells of many attractive monomers densely overlap.

In order to gain more theoretical insight and develop an analytical framework for describing the data, we perform a virial expansion of the transfer free energy $\beta\Delta G \simeq 2B_2^{\text{np}}\phi_n/v_0 + \frac{3}{2}B_3^{\text{np}}(\phi_n/v_0)^2$, and apply it to the partition coefficient $\mathcal{K} = \exp(-\beta\Delta G)$ [84], as

$$\mathcal{K} = \exp \left[-2B_2^{\text{np}} \frac{\phi_n}{v_0} - \frac{3}{2} B_3^{\text{np}} \left(\frac{\phi_n}{v_0} \right)^2 \right], \quad (2)$$

where B_2^{np} is the second virial coefficient, B_3^{np} the third virial coefficient, and $v_0 = \pi\sigma^3/6$ is the network monomer volume with the diameter $\sigma = \sigma_{\text{nn}} = \sigma_{\text{np}}$. The expansion Eq. (2) is compared with the simulation data by fitting the parameters B_2^{np} and B_3^{np} . The final best fits are depicted by the solid curves in Fig. 3a and are in very good agreement. The comparison implies the pronounced contribution of many-body (B_3^{np}) correlations, which are responsible for the non-monotonicity in the attractive and dense regimes.

The fitted B_2^{np} and B_3^{np} parameters can be found in Table I. We find that the second virial coefficients B_2^{np} obtained from the fitting agree

well with the values from the explicit relation $B_2^{\text{np}}(\epsilon_{\text{np}}) = \int_0^\infty dr 2\pi r^2 [1 - \exp(-\beta U_{\text{LJ}}^{\text{np}}(r, \epsilon_{\text{np}}))]$ for LJ particles, cf. Fig. S2a in ESI. However, as shown in Table I and Fig. S2b in ESI, the third virial coefficient B_3^{np} from the fitting deviates from the explicitly computed values of the LJ systems. This implies that as the polymer density increases many-body interactions, including the cross-linkers, play a major role, which is beyond the effect of a simple LJ liquid. In fact, the fitted B_3^{np} values are always positive, *i.e.*, the average many-body effect can be identified as on average a repulsive contribution.

The data in Fig. 3d is also well described by the virial form Eq. (2), where the solid lines agree with the simulation data. For this, we use Eq. (2) with the same virial coefficients obtained from the result in Fig. 3a, and assume $\phi_n = \overline{\phi_n}$, which is in fact a good approximation particularly for low and high polymer densities. The dependence of the partitioning on the network volume fraction can thus again be explained by a balance between the network-penetrant attraction and exclusion, which is particularly important for high volume fractions.

2. Diffusivity

In Fig. 3b the penetrant diffusivity D_{in} in the network is shown versus the polymer packing fraction ϕ_n . Note that the diffusivity is rescaled by the diffusivity in the bulk D_0 . The diffusivity is monotonically decreasing and tends to decay rapidly as the network volume fraction increases [40, 72, 73, 101, 102]. The dashed line depicts $e^{-\phi_n}$ for a simple exponential reference function. We furthermore compare the simulation results with the ‘‘free-volume’’ theory [53, 69, 70, 73, 103–105],

$$D_{\text{in}}^{\text{fv}}/D_0 = b \exp \left[-c \left(\frac{\phi_n}{1 - \phi_n} \right) \right]. \quad (3)$$

The solid lines show the fitting with the prefactor b and the exponent c , which perform in an excellent fashion. The fitting values of b and c are shown in Table I. We note that b decays exponentially as ϵ_{np} increases, while c is rather independent (see Figs. S7 and S8 in ESI for details). This is physically reasonable if we regard diffusion

for large attractions as an activated process, in which the penetrants have to escape from locally bound states ('traps'). Therefore, here we present a semi-empirical scaling expression for the penetrant diffusivity,

$$D_{\text{in}}/D_0 \sim e^{-\beta\epsilon_{\text{np}} - c\left(\frac{\phi_{\text{n}}}{1-\phi_{\text{n}}}\right)}. \quad (4)$$

In Fig. 3e we confirm that $D_{\text{in}}(\epsilon_{\text{np}})$ indeed tends to exponentially decrease. Hence, the Kramers' type scaling $D_{\text{in}} \propto e^{-\beta\epsilon_{\text{np}}}$ for the diffusion limited escape from a single attractive well [72] fits well, such that our prediction from Eq. (4) holds. It is interesting that the energy barrier in the dense systems (*i.e.*, the micro-roughness of the energy landscape) is simply described by ϵ_{np} and not by multiples of it, as we observed in the more ordered systems [84]. Apparently, the random structure (*i.e.*, polydispersity of the network) smoothens out the roughness significantly. Note again that the overall mean attraction (*i.e.*, the mean of the landscape in contrast to its roughness) is much higher than ϵ_{np} , since we needed $7\epsilon_{\text{np}}$ to fit the partition ratio above. We remark that the scaling law Eq. (4) has limitations since it does not behave well when $\phi_{\text{n}} \rightarrow 0$ where D_{in}/D_0 should go to unity. However, this dilute limit with little influence on transport is not interesting anyway for applications and controlling the selectivity. We recall that in literature there are in fact various conventional scaling theories for the diffusivity [72, 73]. In Fig. S7 in ESI, we present several appropriate scaling theories for the diffusivity compared to our simulation results, where Eq. (4) performs the best throughout the range of ϕ_{n} , including the dense regime.

It is interesting that the diffusivity is a simple monotonic function of ϕ_{n} . In fact, this result is very different from our previous finding for regular topologies, that is, membranes made of a fixed (static) fcc (face-centered-cubic) or simple-cubic lattice of LJ spheres [84]. There, we found that the diffusivity is rather a complex function of the density of the membranes. We rationalized the effect by the roughness of a potential landscape, which for ordered potential wells on a regular lattice can be a very rapidly changing function of membrane density in certain density regions [84]. But in the case here, the fluctuations and the polydispersity of the polymer network smoothen out the sharp density effects on the energy landscape and all diffusivities scale similarly exponentially, qualitatively almost independent of the parameter ϵ_{np} .

3. Permeability

In Fig. 3c we present the permeability $\mathcal{P} = \mathcal{K}D_{\text{in}}$ versus the packing fraction. The permeability varies by about 4 orders of magnitude in our parameter range. Due to the generic behavior of the diffusion, the functional form of the permeability reflects essentially the one of the partition ratio \mathcal{K} , while the diffusivity only quantitatively scales the results. Hence, we find that for small interactions ϵ_{np} , the permeability is monotonically decreasing with density, whereas for stronger interactions,

it becomes a non-monotonic function of density. Therefore, as an important finding, the permeability can be maximized in our network model system. For the largest network-penetrant attraction, the permeability is maximized at around $\phi_{\text{n}} \simeq 0.28$ by a factor of around 20 when compared to the bulk reference permeability $\mathcal{P} = D_0$ (the cross symbol).

Having well-performing scaling laws for \mathcal{K} and D_{in} from Eqs. (2) and (4), we attempt to empirically construct also a scaling law for the permeability, via their product, eqn (1),

$$\mathcal{P} = \exp\left[-\beta\epsilon_{\text{np}} - c\left(\frac{\phi_{\text{n}}}{1-\phi_{\text{n}}}\right) - 2B_2^{\text{np}}\frac{\phi_{\text{n}}}{v_0} - \frac{3}{2}B_3^{\text{np}}\left(\frac{\phi_{\text{n}}}{v_0}\right)^2\right], \quad (5)$$

comprising the attractive contribution as a function of the network-penetrant interaction ϵ_{np} , and the exclusion contribution as a function of the packing fraction. The maximization of \mathcal{P} can therefore be understood via Eqs. (2) and (4). The solid lines in Fig. 3c are the predictions from Eq. (5) using the fit parameters determined already in panels a and b, showing very good agreement with the simulation results.

The permeability as a function of the network-penetrant interaction, $\mathcal{P}(\epsilon_{\text{np}})$, shown in Fig. 3f, is an increasing function from the global minimum at around $\beta\epsilon_{\text{np}} = 0.1$, which substantially depends on membrane density. Here, the selective tuning of \mathcal{P} is mainly controlled by the penetrant's excluded volume. The prediction from the empirical scaling Eq. (5) indeed agrees well with the simulation data, in particular, capturing the competition and cancellation between the exponentially growing partitioning and the exponentially decreasing diffusion.

C. Anti-correlations between \mathcal{K} and D_{in} and tuning of the permselectivity

The diagram in Fig. 4 plots partitioning \mathcal{K} versus diffusivity D_{in} and thus presents a landscape visualizing how they are correlated, *i.e.*, a partitioning-diffusivity correlation diagram. The plot shows a wide landscape of the permeability spanning over several orders of magnitude. The black dashed line depicts the iso-permeability line of the bulk permeability $\mathcal{P}/D_0 = 1$, where the two contributions exactly cancel out. The data in Fig. 4 at low and intermediate polymer densities lead to final permeabilities close to the iso-permeability line, hence exhibiting clear anti-correlations and cancellations. Such a cancellation was also observed, even massively leading to more qualitative changes, in membranes constructed by static regular obstacles [84]. This can be understood by going back to our scaling law, Eq. (5). The attraction between monomers and penetrants increases the uptake of penetrants in the membrane roughly exponentially. However, at the same time the attraction enhances the microscopic roughness and deepens local traps, thereby impeding the thermally activated escape, which in turn also leads to an exponential decrease of diffusion. In many regimes,

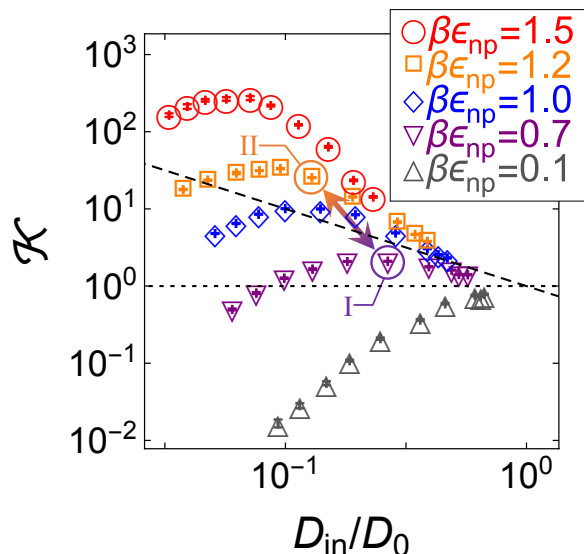


FIG. 4. The partitioning–diffusion \mathcal{K} – D_{in}/D_0 correlation diagram. As depicted in the legend, symbols of the same color have the same network–penetrant interaction, but different polymer densities, *i.e.*, the network–network interaction and hence the polymer volume fraction increases (for each color individually) from right (high diffusion) to the left (low diffusion). The black dashed line depicts the iso-permeability line $\mathcal{P}/D_0 = \mathcal{K}D_{\text{in}}/D_0 = 1$ (reference bulk permeability), where the actions of \mathcal{K} and D_{in} on the membrane permeability exactly cancel each other. The arrow connects two states II ($\beta\epsilon_{\text{np}} = 1.2$) and I ($\beta\epsilon_{\text{np}} = 0.7$) at packing fraction $\phi_n \simeq 0.17$, featuring the selectivity ratio $\alpha_{\text{II,I}} \equiv \mathcal{P}_{\text{II}}/\mathcal{P}_{\text{I}} \simeq 6$, see text.

these two effects cancel out, but the exact behavior depends on the details of the variation of the energy landscape [84]. This can be harvested to tune and optimize the selectivity of a polymer membrane. However, in contrast to the ordered membranes [84], this work indicates that the diffusivity in polydisperse networks only rescales the permeability, while the functional form is dictated by the partitioning behavior.

Hence, the diagram in Fig. 4 presents non-trivial pathways of the permeability \mathcal{P} along the two variable parameters, density and penetrant–network attraction. It clearly shows how the permeability can be tuned substantially over several orders of magnitude already by a relatively small material parameter space. With this, a significant selective permeability (permselectivity) can be demonstrated depending on the interaction parameter ϵ_{np} (which in reality is different for various chemically specific penetrants). For instance, defined as $\alpha_{\text{II,I}} \equiv \mathcal{P}_{\text{II}}/\mathcal{P}_{\text{I}}$ [42], the selectivity for the states II ($\beta\epsilon_{\text{np}} = 1.2$) and I ($\beta\epsilon_{\text{np}} = 0.7$) depicted by the arrow in Fig. 4 at a packing fraction $\phi_n \simeq 0.17$ amounts to $\alpha_{\text{II,I}} \approx 6$, which is large. Hence, a small difference of interactions of half a $k_{\text{B}}T$ results already in a permeability ratio of almost one order of magnitude.

IV. CONCLUSION

We presented extensive (implicit-solvent) coarse-grained simulations and scaling theories for penetrant transport through semi-flexible, cross-linked, and polydisperse polymer networks with a focus on the linear-response permeability, calculated by the equilibrium partitioning and diffusion of the penetrants inside the network. The permeability has been found to be largely tunable by varying the polymer network density and the microscopic interactions between the network and the diffusive penetrants. In particular, significant maximization and minimization of the permeability were found, fine-tuned by the solvent quality and the penetrant–network interactions. The results were rationalized by scaling theories which include a virial expansion with two-body attractions and many-body exclusion effects for the partitioning, and a combination of the free-volume and Kramers’ escape scaling laws for the diffusivity. The presented laws, despite their simplicity, capture salient features of the system, showing good agreement with the simulation results.

The penetrant diffusivity turned out to be rather a smooth function of the network density, implying substantial effects of the fluctuation and randomness of the polymer network. The polydisperse nature of the network averages out the roughness of the energy landscape, which was more pronounced and sensitive to parameter changes in highly ordered, lattice-based and static membrane systems [84]. Nevertheless, the permeability revealed a rather intricate, non-monotonic behavior over several orders of magnitude, originating from the complex nature of the partitioning, while quantitatively and substantially modified by the anti-correlated and canceling contributions of the diffusion. As a consequence, only small changes of interactions, *e.g.*, by half a $k_{\text{B}}T$ can already modify the selectivity of the membrane by a factor of 6. Our study provides a further step in the fundamental understanding and development of a minimal theory to characterize better the permeability in flexible and fluctuating polymer-based membrane systems.

CONFLICTS OF INTEREST

There are no conflicts to declare.

ACKNOWLEDGEMENTS

The authors thank Matthias Ballauff, Benjamin Rotenberg, Arturo Moncho-Jordá and Changbong Hyeon for fruitful discussions. This project has received funding from the European Research Council (ERC) under the European Union’s Horizon 2020 research and innovation programme (grant agreement No. 646659). W.K.K. acknowledges the support by a KIAS Individual Grant (CG076001) at Korea Institute for Advanced

Study. M.K. acknowledges the financial support from the Slovenian Research Agency (research core funding No. P1-0055). The simulations were performed with resources provided by the North-German Supercomputing

Alliance (HLRN). We thank Center for Advanced Computation at the Korea Institute for Advanced Study for providing computing resources for this work.

-
- [1] T. Graham, *Philos. Mag.* **32**, 401 (1866).
- [2] A. Finkelstein, *Water movement through lipid bilayers, pores, and plasma membranes: Theory and reality*, vol. 4 (John Wiley & Sons: New York, 1987).
- [3] Q. Al-Awqati, *Nat. Cell Biol.* **1**, E201 (1999).
- [4] K. P. Lee, T. C. Arnot, and D. Mattia, *J. Memb. Sci.* **370**, 1 (2011).
- [5] R. M. Venable, A. Krämer, and R. W. Pastor, *Chem. Rev.* **119**, 5954 (2019).
- [6] D. Shasby, S. Shasby, J. Sullivan, and M. Peach, *Circ. Res.* **51**, 657 (1982).
- [7] J. Wingender, T. R. Neu, and H.-C. Flemming, in *Microbial extracellular polymeric substances* (Springer, 1999), pp. 1–19.
- [8] E. D. Hay, *Cell biology of extracellular matrix* (Springer Science & Business Media, 2013).
- [9] J. Witten, K. Ribbeck, V. V. Khutoryanskiy, L. Wu, M. Liu, W. Shan, X. Zhu, L. Li, Z. Zhang, and Y. Huang, *Nanoscale* **9**, 8080 (2017).
- [10] C. P. Goodrich, M. P. Brenner, and K. Ribbeck, *Nat. Commun.* **9**, 4348 (2018).
- [11] G. Fuhrmann, *Nat. Nanotechnol.* **15**, 168 (2020).
- [12] J. Taipale and J. Keski-Oja, *FASEB J.* **11**, 51 (1997).
- [13] C. J. Dowd, C. L. Cooney, and M. A. Nugent, *J. Biol. Chem.* **274**, 5236 (1999).
- [14] E. W. Raines, *Int. J. Clin. Exp. Pathol.* **81**, 173 (2000).
- [15] A. M. Garcia, N. Szasz, S. B. Trippel, T. I. Morales, A. J. Grodzinsky, and E. H. Frank, *Arch. Biochem. Biophys.* **415**, 69 (2003).
- [16] R. G. Thorne, A. Lakkaraju, E. Rodriguez-Boulan, and C. Nicholson, *Proc. Natl. Acad. Sci. U.S.A.* **105**, 8416 (2008).
- [17] L. Zhang, B. S. Gardiner, D. W. Smith, P. Pivonka, and A. J. Grodzinsky, *J. Theor. Biol.* **263**, 20 (2010).
- [18] A. D. Theocharis, S. S. Skandalis, C. Gialeli, and N. K. Karamanos, *Adv. Drug. Deliv. Rev.* **97**, 4 (2016).
- [19] A. Halperin, M. Kröger, and F. M. Winnik, *Angew. Chem. Int. Ed.* **54**, 15342 (2015).
- [20] D. M. Vriezema, M. Comellas Aragonès, J. A. A. W. Elemans, J. J. L. M. Cornelissen, A. E. Rowan, and R. J. M. Nolte, *Chem. Rev.* **105**, 1445 (2005).
- [21] S. Carregal-Romero, N. J. Buurma, J. Pérez-Juste, L. M. Liz-Marzán, and P. Hervés, *Chem. Mater.* **22**, 3051 (2010).
- [22] M. A. C. Stuart, W. T. S. Huck, J. Genzer, M. Müller, C. Ober, M. Stamm, G. B. Sukhorukov, I. Szleifer, V. V. Tsukruk, M. Urban, et al., *Nat. Mater.* **9**, 101 (2010).
- [23] Y. Lu and M. Ballauff, *Prog. Polym. Sci.* **36**, 767 (2011).
- [24] K. Renggli, P. Baumann, K. Langowska, O. Onaca, N. Bruns, and W. Meier, *Adv. Funct. Mater.* **21**, 1241 (2011).
- [25] P. Tanner, P. Baumann, R. Enea, O. Onaca, C. Palivan, and W. Meier, *Acc. Chem. Res.* **44**, 1039 (2011).
- [26] Y. Guan and Y. Zhang, *Soft Matter* **7**, 6375 (2011).
- [27] P. Hervés, M. Pérez-Lorenzo, L. M. Liz-Marzán, J. Dzubiella, Y. Lu, and M. Ballauff, *Chem. Soc. Rev.* **41**, 5577 (2012).
- [28] S. Wu, J. Dzubiella, J. Kaiser, M. Drechsler, X. Guo, M. Ballauff, and Y. Lu, *Angew. Chem. Int. Ed.* **51**, 2229 (2012).
- [29] J. Gaitzsch, X. Huang, and B. Voit, *Chem. Rev.* **116**, 1053 (2015).
- [30] S. Campisi, M. Schiavoni, C. Chan-Thaw, and A. Villa, *Catalysts* **6**, 185 (2016).
- [31] G. Prieto, H. Tüysüz, N. Duyckaerts, J. Knossalla, G.-H. Wang, and F. Schüth, *Chem. Rev.* **116**, 14056 (2016).
- [32] S. H. Petrosko, R. Johnson, H. White, and C. A. Mirkin, *J. Am. Chem. Soc.* **138**, 7443 (2016).
- [33] H. Jia, R. Roa, S. Angioletti-Uberti, K. Henzler, A. Ott, X. Lin, J. Möser, Z. Kochovski, A. Schnegg, J. Dzubiella, et al., *J. Mat. Chem. A* **4**, 9677 (2016).
- [34] S. Angioletti-Uberti, Y. Lu, M. Ballauff, and J. Dzubiella, *J. Phys. Chem. C* **119**, 15723 (2015).
- [35] R. Roa, W. K. Kim, M. Kanduč, J. Dzubiella, and S. Angioletti-Uberti, *ACS Catalysis* **7**, 5604 (2017).
- [36] M. Kanduč, W. K. Kim, R. Roa, and J. Dzubiella, *Mol. Syst. Des. Eng.* **5**, 602 (2020).
- [37] L. M. Robeson, *J. Memb. Sci.* **62**, 165 (1991).
- [38] P. Pandey and R. Chauhan, *Prog. Polym. Sci.* **26**, 853 (2001).
- [39] E. Atci, I. Erucar, and S. Keskin, *J. Phys. Chem. C* **115**, 6833 (2011).
- [40] K. Falk, B. Coasne, R. Pellenq, F.-J. Ulm, and L. Bocquet, *Nat. Commun.* **6**, 6949 (2015).
- [41] A. Obliger, R. Pellenq, F.-J. Ulm, and B. Coasne, *J. Phys. Chem. Lett.* **7**, 3712 (2016).
- [42] B. D. Freeman, *Macromolecules* **32**, 375 (1999).
- [43] H. B. Park, J. Kamcev, L. M. Robeson, M. Elimelech, and B. D. Freeman, *Science* **356**, 1137 (2017).
- [44] M. A. Shannon, P. W. Bohn, M. Elimelech, J. G. Georgiadis, B. J. Mariñas, and A. M. Mayes, *Nature* **452**, 301 (2008).
- [45] G. M. Geise, H.-S. Lee, D. J. Miller, B. D. Freeman, J. E. McGrath, and D. R. Paul, *J. Polym. Sci. B* **48**, 1685 (2010).
- [46] G. M. Geise, H. B. Park, A. C. Sagle, B. D. Freeman, and J. E. McGrath, *J. Memb. Sci.* **369**, 130 (2011).
- [47] D. Menne, F. Pitsch, J. E. Wong, A. Pich, and M. Wessling, *Angew. Chem. Int. Ed.* **53**, 5706 (2014).
- [48] B. Tansel, J. Sager, T. Rector, J. Garland, R. F. Strayer, L. Levine, M. Robert, M. Hummerick, and J. Bauer, *Sep. Purif. Technol.* **51**, 40 (2006).
- [49] Z. Tan, S. Chen, X. Peng, L. Zhang, and C. Gao, *Science* **360**, 518 (2018).
- [50] W. Hyk and K. Kitka, *J. Environ. Chem. Eng.* **6**, 6108 (2018).
- [51] C. S. Brazel and N. A. Peppas, *Polymer* **40**, 3383 (1999).
- [52] D. F. Stamatialis, B. J. Papenburg, M. Girones, S. Saiful, S. N. Bettahalli, S. Schmitmeier, and M. Wessling,

- J. Memb. Sci. **308**, 1 (2008).
- [53] H. Yasuda, A. Peterlin, C. Colton, K. Smith, and E. Merrill, *Die Makromol. Chemie* **126**, 177 (1969).
- [54] D. R. Paul, *Separation and Purification Methods* **5**, 33 (1976).
- [55] J. Williams and R. W. Baker, *J. Memb. Sci.* **107**, 1 (1995).
- [56] S. Gehrke, J. Fisher, M. Palasis, and M. E. Lund, *Ann. N. Y. Acad. Sci.* **831**, 179 (1997).
- [57] S. C. George and S. Thomas, *Prog. Polym. Sci.* **26**, 985 (2001).
- [58] M. Ulbricht, *Polymer* **47**, 2217 (2006).
- [59] A. Missner and P. Pohl, *Chem. Phys. Chem* **10**, 1405 (2009).
- [60] R. W. Baker and B. T. Low, *Macromolecules* **47**, 6999 (2014).
- [61] A. Obliger, M. Jardat, D. Coelho, S. Bekri, and B. Rotenberg, *Phys. Rev. E* **89**, 043013 (2014).
- [62] A. Moncho-Jordá and I. Adroher-Benítez, *Soft Matter* **10**, 5810 (2014).
- [63] I. Adroher-Benítez, S. Ahualli, A. Martín-Molina, M. Quesada-Pérez, and A. Moncho-Jordá, *Macromolecules* **48**, 4645 (2015).
- [64] A. Erbaş and M. Olvera de la Cruz, *Macromolecules* **49**, 9026 (2016).
- [65] B. Rotenberg, J.-F. Dufreche, B. Bagchi, E. Giffaut, J.-P. Hansen, and P. Turq, *J. Chem. Phys.* **124**, 154701 (2006).
- [66] W. K. Kim, A. Moncho-Jordá, R. Roa, M. Kanduč, and J. Dzubiella, *Macromolecules* **50**, 6227 (2017).
- [67] L. Pérez-Mas, A. Martín-Molina, M. Quesada-Pérez, and A. Moncho-Jordá, *Phys. Chem. Chem. Phys.* **20**, 2814 (2018).
- [68] M. Kanduč, W. K. Kim, R. Roa, and J. Dzubiella, *ACS nano* **13**, 11224 (2019).
- [69] H. Yasuda, C. Lamaze, and L. D. Ikenberry, *Die Makromol. Chemie* **118**, 19 (1968).
- [70] H. Yasuda, L. Ikenberry, and C. Lamaze, *Die Makromol. Chemie* **125**, 108 (1969).
- [71] I. C. Kim and S. Torquato, *J. Chem. Phys.* **96**, 1498 (1992), ISSN 00219606.
- [72] L. Masaro and X. Zhu, *Prog. Polym. Sci.* **24**, 731 (1999).
- [73] B. Amsden, *Macromolecules* **31**, 8382 (1998).
- [74] A. P. Chatterjee, *J. Phys. Condens. Matter* **23**, 375103 (2011).
- [75] Y. Jiao and S. Torquato, *Phys. Biol.* **9**, 036009 (2012).
- [76] M. Spanner, S. K. Schnyder, F. Höfling, T. Voigtmann, and T. Franosch, *Soft Matter* **9**, 1604 (2013).
- [77] A. Godec, M. Bauer, and R. Metzler, *New J. Phys.* **16**, 092002 (2014).
- [78] H. Liasneuski, D. Hlushkou, S. Khirevich, A. Höltzel, U. Tallarek, and S. Torquato, *J. Appl. Phys.* **116**, 034904 (2014).
- [79] X. Zhang, J. Hansing, R. R. Netz, and J. E. DeRouchey, *Biophys. J.* **108**, 530 (2015).
- [80] J. Hansing, C. Ciemer, W. K. Kim, X. Zhang, J. E. DeRouchey, and R. R. Netz, *The Eur. Phys. J. E* **39**, 53 (2016).
- [81] J. Hansing, J. R. Duke III, E. B. Fryman, J. E. DeRouchey, and R. R. Netz, *Nano Letters* **18**, 5248 (2018).
- [82] J. Hansing and R. R. Netz, *Macromolecules* **51**, 7608 (2018).
- [83] J. Hansing and R. R. Netz, *Biophys. J.* **114**, 2653 (2018).
- [84] W. K. Kim, M. Kanduč, R. Roa, and J. Dzubiella, *Phys. Rev. Lett.* **122**, 108001 (2019).
- [85] P. Jha, J. Zwanikken, F. Detcheverry, J. de Pablo, and M. Olvera de la Cruz, *Soft Matter* **7**, 5965 (2011).
- [86] M. Quesada-Pérez, J. Ramos, J. Forcada, and A. Martín-Molina, *J. Chem. Phys.* **136**, 244903 (2012).
- [87] P. Košován, T. Richter, and C. Holm, *Macromolecules* **48**, 7698 (2015).
- [88] H. Kobayashi and R. G. Winkler, *Sci. Rep.* **6**, 19836 (2016).
- [89] A. Schmid, J. Dubbert, A. A. Rudov, J. Pedersen, P. Lindner, M. Karg, I. Potemkin, and W. Richtering, *Sci. Rep.* p. 22736 (2016).
- [90] I. Zadok and S. Srebnik, *J. Phys. Chem. B* **122**, 7091 (2018).
- [91] M. Kanduč, W. K. Kim, R. Roa, and J. Dzubiella, *Macromolecules* **51**, 4853 (2018).
- [92] P. Higgs and R. Ball, *J. Phys. France* **49**, 1785 (1988).
- [93] E. Geissler, F. Horkay, and A.-M. Hecht, *Phys. Rev. Lett.* **71**, 645 (1993).
- [94] G. Glatting, R. Winkler, and P. Reineker, *Macromolecules* **28**, 5906 (1995).
- [95] J. S. Soares and P. Zunino, *Biomaterials* **31**, 3032 (2010).
- [96] S. Plimpton, *J. Comp. Phys.* **117**, 1 (1995).
- [97] H. J. C. Berendsen, J. P. M. Postma, W. F. van Gunsteren, A. DiNola, and J. R. Haak, *J. Chem. Phys.* **81**, 3684 (1984).
- [98] J. Heyda, A. Muzdalo, and J. Dzubiella, *Macromolecules* **46**, 1231 (2013).
- [99] S. Milster, R. Chudoba, M. Kanduč, and J. Dzubiella, *Phys. Chem. Chem. Phys.* **21**, 6588 (2019).
- [100] J. Shin, A. G. Cherstvy, W. K. Kim, and V. Zaburdaev, *Phys. Chem. Chem. Phys.* **19**, 18338 (2017).
- [101] J. Haus and K. Kehr, *Phys. Rep.* **150**, 263 (1987).
- [102] S. K. Ghosh, A. G. Cherstvy, and R. Metzler, *Phys. Chem. Chem. Phys.* **17**, 1847 (2014).
- [103] N. A. Peppas and C. T. Reinhart, *J. Memb. Sci.* **15**, 275 (1983).
- [104] C. T. Reinhart and N. A. Peppas, *J. Memb. Sci.* **18**, 227 (1984).
- [105] S. R. Lustig and N. A. Peppas, *J. Appl. Polym. Sci.* **36**, 735 (1988).